

Quantification of Cellular Properties from External Fields and Resulting Induced Velocity: Cellular Hydrodynamic Diameter

Jeffrey J. Chalmers,¹ Seungjoo Haam,^{1,*} Yang Zhao,¹ Kara McCloskey,¹ Lee Moore,² Maciej Zborowski,² P. Stephen Williams³

¹Department of Chemical Engineering, The Ohio State University, 140 West 19th Avenue, Columbus, Ohio 43210; telephone: +1 (614) 292-2727; fax: +1 (614) 292-3769; e-mail: Chalmers.1@osu.edu

²Department of Biomedical Engineering, The Cleveland Clinic Foundation, 1900 Euclid Avenue, Cleveland, Ohio 44195

³Department of Chemistry and Geochemistry, Colorado School of Mines, 1500 Illinois Street, Golden, Colorado 80401

Received 16 May 1998; accepted 11 January 1999

Abstract: An experimental technique is discussed in which the size distribution of a population of cells is determined by calculating each cell's settling velocity. The settling velocity is determined from microscopically obtained images which were recorded on SVHS tape. These images are then computer imaged and processed, and the cell's location and velocity are determined using a computer algorithm referred to as cell tracking velocimetry (CTV). Experimental data is presented comparing the distribution of human lymphocytes and a human breast cancer cell line, MCF-7, determined using a Coulter counter and the CTV approach. © 1999 John Wiley & Sons, Inc. *Biotechnol Bioeng* 64: 509–518, 1999.

Keywords: image analysis; cell diameter; cell tracking velocimetry

INTRODUCTION

The ability to analyze and separate a heterogeneous cell population based on cellular characteristics is a significant analytical and preparative resource. These characteristics range from cell size to the presence of specific cell surface markers or molecules on either the surface or within the cell. The actual instruments used in cell analysis or separation range from relatively simple devices to highly complex ones. Systems include the relatively simple centrifuges or membranes to moderately complex devices, such as Coulter counters, to the highly complex and expensive fluorescence-activated cell scanners/sorters (FACS). Central to all these devices is the instrument's ability to exploit a unique, specific cellular attribute which either is intrinsic to the cell

(such as cell size) or added to the cell (such as a specific fluorescent probe). This exploitation of the cellular attribute involves its identification in the case of analysis or its use as a "handle" in the case of separation. Typically, the instrument imposes on the cell suspension a field, such as gravity, centrifugal, magnetic, pressure, or electric. In some cases the instrument imposes on the cell suspension a specific energy "beam" as in a light beam of a specific wavelength (laser). The instrument then records or detects how the cellular attribute interacts with this imposed field or beam.

With respect to cell size analysis, a number of different cellular attributes have been used to calculate cell size. These attributes include: actual physical size differences, density differences, electrical conductivity differences, and differences in forward angle light scattering (FALS). The degree of complexity and accuracy of these methods starts with relatively simple membrane filtration systems and extends to highly sophisticated FACS systems using FALS.

An example of an instrument that uses electrical conductivity differences is a Coulter counter. This instrument is regularly used to measure both cell concentrations and cell size distributions. It is based on the Coulter principle which measures both the presence and size of a cell by detecting changes in impedance of an electrolyte solution containing the cells to be analyzed as they flow through a small orifice in the instrument.

Because of the widely successful applications of FACS systems, forward angle light scattering (FALS) is widely used to determine cell sizes. FALS is based on the principle that the degree to which a laser beam is scattered when the beam encounters a particle is proportional to the particle cross-sectional area. FALS is routinely used in FACS systems to differentiate between lymphocytes and monocytes, a difference in diameter of approximately 2 μm (Bikoue et al., 1996). However, there are reports in which FALS can give false values. For example, Shapiro (1995) reports on a

* Present address: Chemical Engineering Department, Yonsei University, 134 Shinchon-Dong, Seodaemoon-Ku, Seoul 120-752, Korea

Correspondence to: J. J. Chalmers

Contract grant sponsors: National Science Foundation; National Institutes of Health; Whitaker Foundation

Contract grant numbers: BCS 9258004; CA 62349; 20010308

case in which electronic volume measurements of blood granulocyte indicate that their volume (350 fl) is greater than the volume of lymphocytes (200 fl); yet granulocytes produce a smaller FALS than lymphocytes in some FACS, indicating that granulocytes are smaller. A number of factors affect FALS, including wavelength of light used, range of angles over which light is collected, refractive index between the cell and suspending medium, and cell internal structure. Even with most of the variables above held constant, it has been shown that the relationship between FALS and cell diameter can be highly nonlinear (Terstappen, 1990).

In addition, personal communications with a major producer of FACS systems indicates that size reported by FACS systems can be a distortion of the true cell size. This distortion is believed to be a result of the distortion of the shape of the cells due to the formation and ejection of the liquid drop containing the cell before it is illuminated by the laser. This distortion can result in a larger distribution in cell size than is actually true of the cell populations. This effect is hidden since the typical method of calibration of FACS uses solid beads. The rigid beads would not be subject to distortion as a cell would. Consequently, while a very good correlation between FACS and bead size can be obtained, the same is not necessarily true for cells. Finally, another significant limitation of FACS systems with respect to measuring cell size is that large cells are often destroyed in the drop ejection process, thus limiting the FACS to small cells.

Two commercial devices that can be used for both cell size analysis and separation are unit gravity sedimentation and counterflow centrifugation (or centrifugal elutriation). The first device is based on gravity, while the second device relies on a balance between centrifugal sedimentation and centripetal flow (Bertoncello, 1987). With respect to unit gravity sedimentation, the terminal velocity, v_t , is given by

$$v_t = \frac{2(\rho_c - \rho)gr_c^2}{9\eta}, \quad (1)$$

where ρ_c and ρ are the density of the cell and media, respectively, g is the acceleration due to gravity, r_c is the radius of a cell, and η is the viscosity of the media. If one assumes that a cell is a perfect sphere and that the cell density is constant, one can simplify Eq. (1) to

$$v_t = kV^{2/3}, \quad (2)$$

which indicates that the cell volume (or radius) is the major factor determining the settling velocity and correspondingly, the system's ability to separate the cells.

With respect to centrifugal elutriation, the settling velocity is given by

$$v_t = \frac{(\rho_c - \rho)V\omega^2 r}{2\eta K_1 r_c}, \quad (3)$$

where ω is the angular velocity, r is the radial distance from the center of rotation to the cell, and K_1 is a cell shape factor.

Since both of these separation techniques (unit gravity

Table I. Approximate volumes and densities in isotonic media of typical mammalian cells (from Meistrich, 1983).

Cell type	Volume (μm^3)	Density (g/cm^3)	Density difference ^a ($\rho_c - \rho$)
Erythrocyte	50	1.090	0.074
Small lymphocyte	120	1.075	0.059
Polymorphonuclear leukocyte	200	1.080	0.064
Monocyte	400	1.063	0.047
Macrophage	800	1.050	0.034
Pachytene spermatocyte	2200	1.046	0.030
Round spermatid	600	1.043	0.027
Spermatozoon	20	1.100	0.084

^aA medium density of $1.016 \text{ g}/\text{cm}^3$ was used.

sedimentation and centrifugal elutriation) use a form of sedimentation velocity to differentiate different cell types, a fundamental assumption is that the cell density does not vary from cell to cell in a given sedimentation subpopulation. Eqs. (1) and (3) both indicate that the settling velocity is directly proportional to the difference between the cell density and that of the suspending medium. Between different cell types, significant differences in both cell diameter and density exist. Table I, taken from Meistrich (1983), lists the approximate cell sizes and densities of several types of mammalian cells suspended in isotonic media. As can be observed, a very large difference in cell volume exists in this set of data, 50–2200 μm^3 , or 2.285–8.068 μm cell radius (if a perfect sphere is assumed), but the densities only range from 1.043 to 1.10 g/cm^3 , which is a difference of about 5.5%. However, when one considers the density difference ($\rho_c - \rho$) a larger difference, ranging from 0.027 to 0.084, or a factor of 3.1, is observed. A more specific comparison of cell sizes and densities was conducted by Lasky and Zanjani (1985) on human peripheral blood and bone marrow samples. In this study, size and density of committed colony-forming units–granulocytes, macrophages (CFU-GM), blast-forming units–erythrocytes (BFU-E), colony-forming units–erythrocytes (CFU-E), and multipotent (CFU-MIX) hematopoietic progenitor cells were determined. Two experimental techniques were used: centrifugal elutriation and Percoll gradient, for cell size and density, respectively. Table II, compiled from the work of Lasky and Zanjani (1985), presents cell source, cell type based on cell growth studies, elutriation flow rate for the specific cell fraction of interest, calculated cell size, and density of the cells in that specific fraction. As can be observed, within a specific fraction, the variability of the cell size and density is relatively small.

This paper is the first of a two-part sequence in which we will discuss our use of a specific computer imaging procedure, cell tracking velocimetry (CTV), and of a natural external field, gravity, to determine cell size by calculating settling velocities of large numbers of cells. In the second paper, we will discuss the use of CTV, with an applied magnetic energy gradient, to determine the magnetic sus-

Table II. Calculated cell size and density of committed and multipotent hematopoietic progenitors cells from peripheral blood and bone marrow (Lasky and Zanjani, 1985).

Source	Cell type	Elutriation fraction (ml/min, mean + SE)	Cell diameter (μm)	Cell density (g/cm^3 , mean + SE)
Marrow	CFU-MIX	14.3 ± 0.7	8.59	1.0666 ± 0.0020
Blood	CFU-MIX	14.7 ± 0.2	8.72	1.0625 ± 0.0014
Marrow	BFU-E	14.3 ± 0.7	8.59	1.0641 ± 0.0017
Blood	BFU-E	14.7 ± 0.2	8.72	1.0625 ± 0.0014
Marrow	CFU-GM	15.7 ± 0.7	8.97	1.0666 ± 0.0020
Blood	CFU-GM	14.7 ± 0.2	8.72	1.0632 ± 0.0009
Marrow	CFU-E	18.3 ± 0.7	9.69	1.0762 ± 0.0041

ceptibility of immunomagnetically labeled cells. If it is assumed that a proportionality exists between the magnetic susceptibility of an immunomagnetically labeled cell and the number of cell surface markers, then this approach can be used to determine the total number of cell surface markers expressed on the cell surface.

MATERIALS AND METHODS

Cells Used and Cell Preparation

Two types of cells were used for this study: human lymphocytes and the 2C4 cell line, which was derived from human fibrosarcoma HT1080 cells.

Human Lymphocytes

Human lymphocytes were obtained from apparently healthy donors in accordance with the Cleveland Clinic Foundation (CCF) Institutional Review Board (IRB). The cells were obtained from peripheral blood through vein puncture. The Ficoll–Paque technique was used to obtain peripheral blood mononuclear (PBMN) cells by layering diluted blood over a Ficoll–Paque cushion (density of 1.077; Pharmacia, Uppsala, Sweden), centrifuging, and collecting cells at the interface. These cells were then suspended in PBS buffer before being analyzed for cell settling velocity.

2C4 Cell Line

The 2C4 cell line, generously provided by Dr. George Stark, Cleveland Clinic Foundation, was derived by stable co-transfection of human fibrosarcoma HT1080 cells with pDW9-27 CD2 and pTK-Neo vectors (Watling et al., 1993; Han et al., 1997). These cells are grown in DMEM medium (Gibco-BRL; cat. no. 11995-065) supplemented with 10% FCS and $1 \times$ penicillin–streptomycin. For cell settling experiments, the cells were suspended in PBS buffer.

Cell Size Determination

Two different types of Coulter counters (Coulter Corporation, Miami, FL) have been used in our laboratories to determine total cell number and size distributions: a Model Z1 and a Multisizer IIe. To obtain a histogram of cell sizes with the Model Z1, the operator had to manually select the window size and range, or “bin”, of interest. In the results using the Z1 presented below, a total of 48 increments were chosen, each $0.5 \mu\text{m}$ wide, ranging from 5.125 to $19.25 \mu\text{m}$. The second Coulter counter, the Multisizer IIe, automatically records the data with a bin size without manually selecting window size. Both instruments used a $100\text{-}\mu\text{m}$ aperture in the sampling electrode.

Experimental Apparatus

The same experimental apparatus, with minor modifications, as was used by Reddy et al. (1996) was used in this study. Figure 1a, taken from Reddy et al. (1996), presents a perspective view of the system. Cells, either immunomagnetically labeled or unlabeled as in this study, are pumped through tubing into the channel. This square, borosilicate glass channel (nominally $1 \text{ mm I.D.} \times 1.4 \text{ mm O.D.}$) is placed on the surface of the magnetic pole pieces, and the region of analysis is highlighted.

As a control experiment to determine if the magnetic energy field has an effect on the settling velocity of cells, a system was used in which the magnetic pole pieces were replaced with a sheet of black painted steel to which the

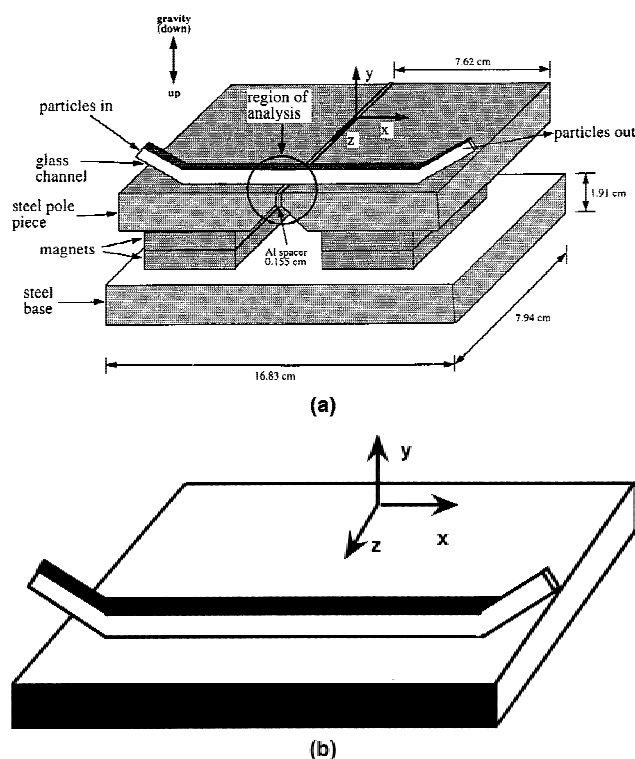


Figure 1. Schematic diagram of the experimental apparatus.

glass column was attached (Fig. 1b). Otherwise, this system was identical to the one containing the magnets.

Imaging System

Cell movement was observed with an Olympus BHMJ microscope using a 5× objective. Light was supplied internally through the microscope by a Fiber Lite (Dolan-Jenner, Lawrence, MA) fiber optic light source without the fiber optic cable. A Cohu (San Diego, CA) CCD 4915 camera which operated on 30-Hz framing speed and a Sony SVO-9500MD SVHS video recorder were used to record cell movement. A 2.5× or 6.7× magnification photoeyepiece was used.

Analysis of Experimental Data: Computer Imaging and Analysis of Cell Velocity

To obtain a large amount of quantitative data on cell location and velocity, the SVHS recorded images were analyzed using a procedure outlined in Fig. 2. Once digitized, the images were processed into a standardized form to facilitate the task of determining the location of the cells. Next, a computer algorithm referred to as cell tracking velocimetry (CTV), processed the data. This CTV algorithm is a modification of the computer algorithm, particle tracking velocimetry (PTV), developed by Dr. Y. Guezenec and R. Brodkey of the Departments of Mechanical and Chemical Engineering at The Ohio State University. The PTV algorithm can determine the three-dimensional location and velocity of up to 1000 particles per frame from five consecutive stereoscopic images (Guezenec et al., 1994). Each image processing step is discussed below.

Image Acquisition/Digitization

Microscopically acquired images were recorded by a CCD camera using SVHS VCR format. Cell suspensions to be analyzed were pumped into the apparatus, and the velocity due to this pumping was allowed to stop before images of the cells settling (in a direction perpendicular to the pumping direction) was recorded. A DIPIX P360F image board (DIPIX technology Inc, Canada) was used to convert the analog VCR image into a 624 × 450 pixel array of 8 bits of gray level information ranging from 0 (black) to 255 (white) for each pixel. The actual image acquisition by the computer was automated using a program written in Borland C++ using a RS-232C interface with the VCR. This program is capable of pinpointing a frame number of interest and activating the DIPIX image grabber to digitize the images automatically. An SVGA graphic card with a resolution up to 1280 × 1024 and 256 gray levels and Borland C++ based software were used for image display on the PC. An example of a raw, digitized image is shown in Fig. 3a.

Image Processing

Image processing is the image enhancement step used to improve the digitized images prior to the identification and

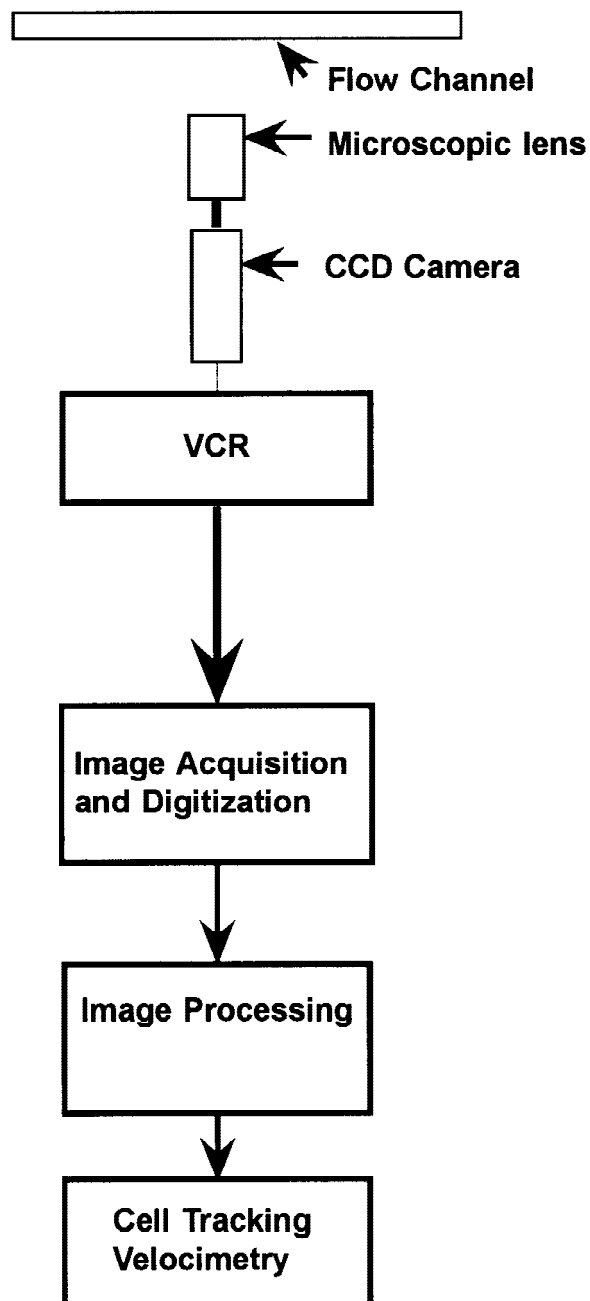


Figure 2. Flow sheet of procedure used to acquire and analyze images of moving cells.

tracking of the cells using the CTV algorithm. The specific image processing steps were histogramming, stretching, background image, low pass filtering, subtraction, and size filtering.

Histogramming. The statistical technique of histogramming is used to determine the appropriate image processing for optimal image enhancement. Histogramming, in the context of image processing, is a measure of the frequency of various gray levels in an image. By careful examination of the raw image in Fig. 3a, one can observe that the cells in focus have both dark and light regions, while the out of focus cells are purely dark. This observation is quantita-

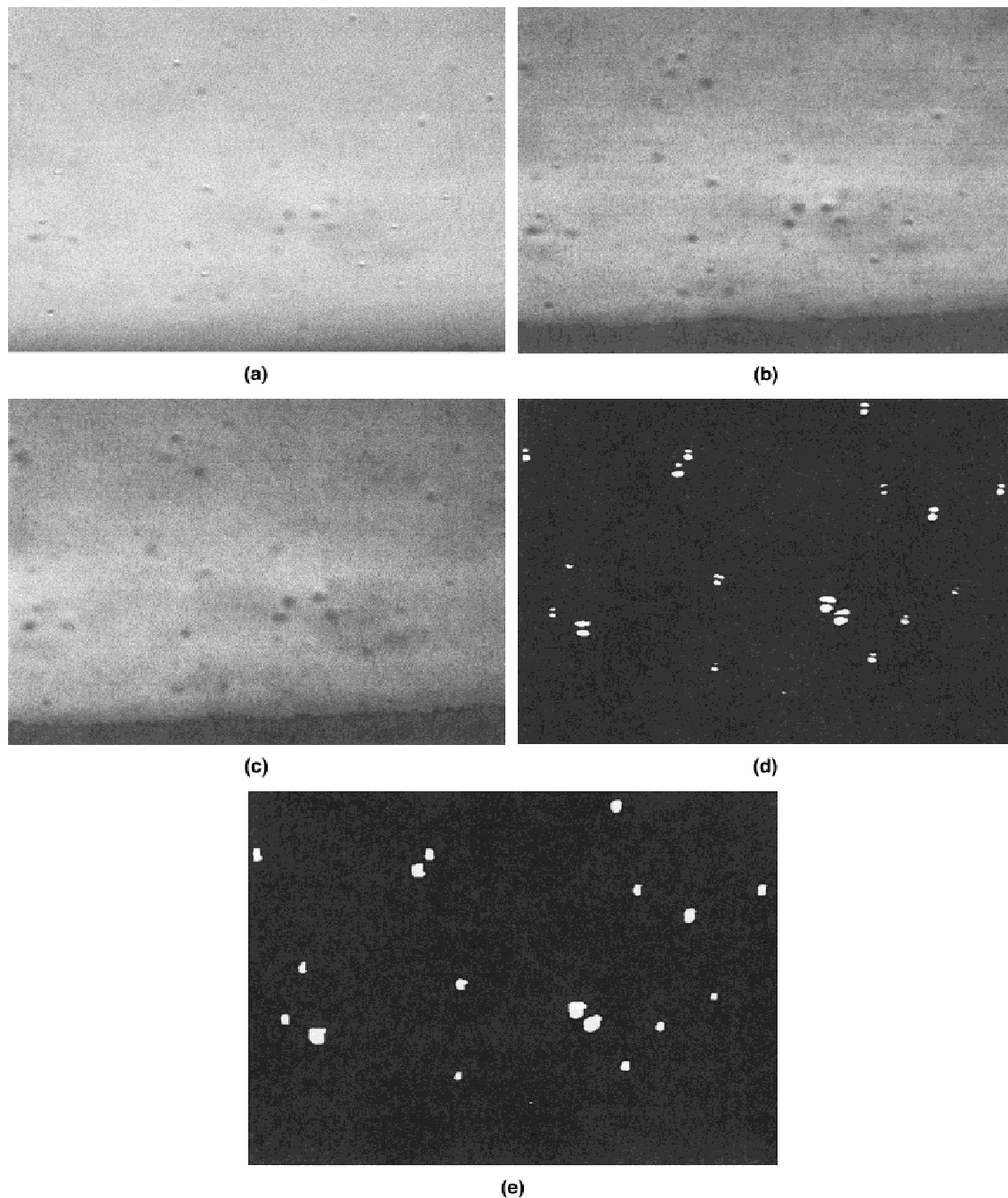


Figure 3. Examples of various forms of a digitized image of cells in the experimental device ($6.7\times$ eyepiece). (a) Raw image, after being initially digitized from an SVHS recording. (b) Stretched version of a. (c) Low pass filtered version of b. (d) Image c after background subtraction. (e) Image after the second filtering process.

tively demonstrated in the histogram of Fig. 3a presented in Fig. 4a. As Fig. 4a demonstrates, cell images occur at both ends of the histogram. This observation adds significant complexity to the image processing.

Stretching. The stretching process is commonly used when the distribution of the gray level in the image does not cover the full brightness range and produces poor contrast between the object of interest and the background. This process is done after the range of the gray level is found by histogramming. Stretching is made by setting two values: a

minimum and a maximum. In this process, all the pixels with intensity less than the minimum values are set to zero (black) and those with intensity greater than the maximum values are set to 255 (white). The pixels with the intensities in the range between the minimum and maximum values are stretched proportionally to their original intensity. For 8-bit resolution, this is between 0 and 255. The minimum and maximum values are carefully selected by the user, and the stretched image contains more distinct peaks (distributions) corresponding to the cells and the background. Figure 3b

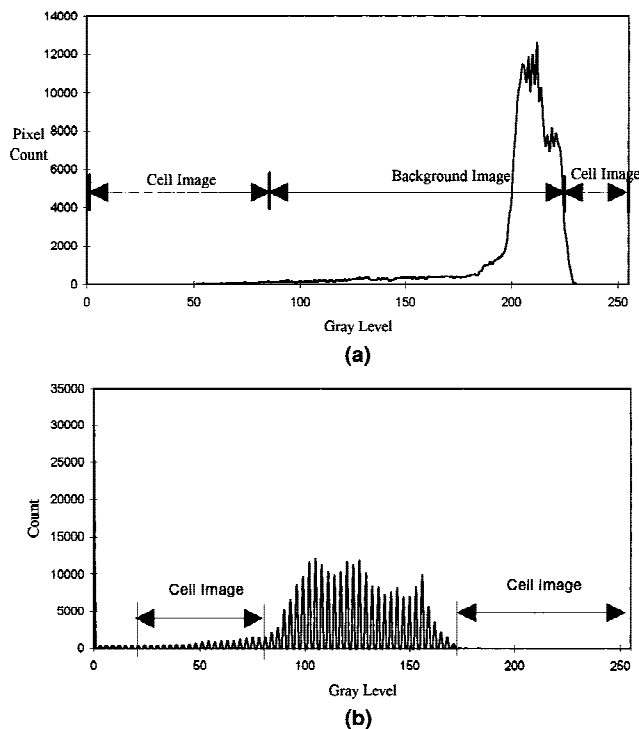


Figure 4. Histograms of the gray levels of the pixels in Figs. 3a and 3b, respectively.

shows the quality of the enhanced image using the stretching process. The gray level histogram of the stretched image is also shown in Fig. 4b.

Low pass spatial filtering. Low pass spatial filter is used in image processing steps such as removal of small details (noise) from an image. A low pass spatial filter is often called “neighborhood averaging” and is used to reduce noise by smoothing local gray levels of an image. The low pass spatial filtered image is shown in Fig. 3c.

Background subtraction. The CTV technique requires an image containing only dark background and bright cells. However, the experimental system does not create such an image. In our application, the experimental system includes additional objects such as part of a magnet, the edge of the glass channel, microscopic debris, etc. The subtraction process can remove this background by subtracting the raw image containing only the background from the raw images that contain the cells. In Fig. 3d the background noise of the low pass filtered image was removed by subtraction.

Filtering based on the pattern and pixel size matching. From Fig. 3d it can be observed that the cell images can appear as hollow spheres or elliptical objects since the core of the cells have the same gray level as background, and there are still small amounts of noises left. To overcome this incomplete cell image, a standard complete cell image is artificially made and used as a template. The cell images in Fig. 3d are compared to the template and are reconstructed as complete cell images if the pattern sizes match. A sample image after this filtering process is shown in Fig. 3e.

Cell Tracking Velocimetry, CTV. This processing step

consists of two parts: determination of cell location and 2D tracking. Cell locations are identified based on the contrast difference of the object from the background. The cell itself is defined as an arbitrary shape and size connected by a set of pixels with an intensity exceeding a given threshold value, and the shape itself is defined by the user. Defined cell parameters include the minimum and maximum size and aspect ratio (which determines shape). The cell identification and location algorithm scans the pixels of the image and identifies the cell and labels the location at the center of a cell based on user defined parameters.

The 2D tracking module uses a sequence of five frames to establish the most probable path (as a function of time) taken by each of these cells. The tracks are determined based on the concept of path coherence. The idea behind this concept is that cell position, velocity, acceleration, and change of acceleration are internally self consistent and that they can be described by smooth functions.

Starting with a cell in the first frame, a search radius is established, and all cells within the search radius in the second frame are tagged. The procedure is repeated for the 3rd, 4th, and 5th subsequent frames. Therefore, the size of the tree grows geometrically as the number of frames increases. Each of the various candidates’ paths is evaluated for the path coherence. From the first two frames, the path of the cell in the third frame is determined by using backward finite difference approximation and then compared to the actual position in the third frame. After comparison, the error of distance from the predicted and the actual cell position is added to the penalty function. The procedure is repeated for the fourth frame using the first three frames and, similarly, for the fifth frame. The process is reversed from the fifth, back to the first, to eliminate any biases. The value of the penalty functions is analyzed for the various cell tracks, and the one with the minimum penalty function is chosen as the path. This technique is very reliable and fully automated. The original PTV algorithm does not identify specific cells (particles) through a series of video frames since the algorithm was developed for 3D flow visualization studies in which instantaneous velocities of hundreds of particles are desired. Consequently, it was modified to provide specific cells tracks and velocities through a series of frames for this application. See the following references for further discussion the PTV methodology and applications: Guezennec et al. (1994); Reddy et al. (1996); and Venkat et al. (1996).

RESULTS

Coulter Counter Analysis of Cell Diameter, Human Lymphocytes

In our laboratories (Zborowski and Chalmers) we have been using the Ficoll–Paque-separated human lymphocytes for immunomagnetic cell separation studies for a number of years (Chalmers et al., 1998; Sun et al., 1998; Zborowski et al., 1997, 1995). Figure 5a presents a typical histogram, using solid bars, of the size distributions of these separated

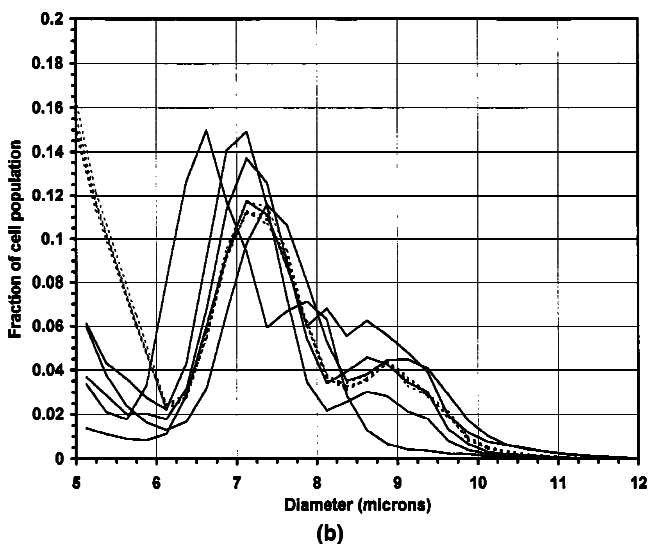
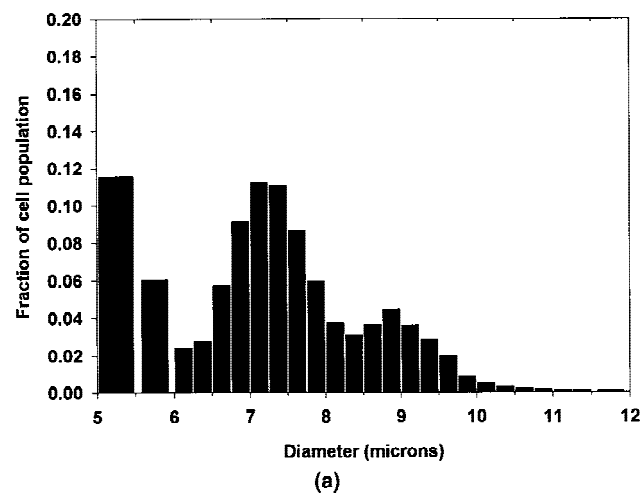


Figure 5. (a) Histogram, from Z1 Coulter counter data, of the fraction of cell population with a given cell diameter, normalized to the total cell count, for Ficoll–Paque-separated human blood. (b) X–Y plot of a total of ten analyses using the Z1 Coulter Counter from six donors. Each of the thin, solid lines corresponds to a unique donor, while the dotted lines correspond to five experiments using the same donor cells. The thick solid line corresponds to the average of all ten runs.

lymphocytes determined using the Model Z1 Coulter counter. To determine the reproducibility of the Ficoll–Paque separation technique and the Z1 counter, a total of ten different size distribution experiments using the Z1 were conducted. Of the ten size experiments conducted, five of the cell suspension samples came from different donors, and five additional size experiments were conducted on cells from a single donor. To allow all ten of these size experiments to be plotted on the same graph, the histogram “bars” were replaced with lines. The five single-size determinations, each from a different donor, are presented as light, solid lines in Fig. 5b, while the cell sample that was tested five times (one donor) is presented as dotted lines. As can be observed, significant variability was obtained in the cells from donor to donor, but the cells from the single donor tested five times produced almost identical results. The tail

end of a large peak observed at the left side of the histogram is most probably the result of a combination of red blood cells and cellular debris. The primary peak at approximately 7 μm is the lymphocyte population, and the smaller shoulder around 8.8 μm is most probably the result of the presence of monocytes. These conclusions are consistent with the manufactures’ information regarding the Ficoll–Paque separation performance. Table III presents the number of cells analyzed and the diameter of the lymphocyte peak for each of the ten runs presented in Fig. 5.

Figure 6 presents the results of three consecutive (the same cell sample) size determination runs of fibrosarcoma 2C4 cells in the Multisizer IIe. The dotted line is the result of each run while the solid line is the average of the three. Table IV presents the number of cells analyzed, the mean diameter, and the standard deviation. These statistics were determined by the Coulter counter software using a window between 9.77 and 29.81 μm and a “bin” size of 0.25 μm . This range was chosen on the basis of visual observation of the histogram created by the instrument software.

Determination of Settling Velocity Using the Device and Computer Algorithms

The final output from the CTV algorithm is a matrix of data with each row of data corresponding to an individually tracked cell in a specific frame, and each column of the matrix corresponding to the x and y location and the u and v components of the velocity vector of the tracked particle. After examination of the data, a condition was established such that the velocity for a specific cell had to be determined for at least 10 consecutive frames before an average of the settling velocity of that cell was reported.

Figures 7 and 8 are histograms of the fraction of cell populations with a given settling velocity versus the cell settling velocity (mm/s), on a log scale, for human lymphocytes and 2C4 cells, respectively. Ten bins per decade, distributed in a logarithmic manner, were used. Table V presents the number of cells analyzed, and the mean and standard deviation (calculated using a linear scale) of the

Table III. Results of Coulter counter (Model Z1) analysis of Ficoll–Paque-separated human lymphocytes; runs 1–5 are from different donors, while runs 5–10 are repeated analyses of the same donor sample.

Run no.	No. of cells analyzed	Diameter of lymphocytes peaks (microns)
1	79,840	7.38
2	149,964	6.63
3	370,980	7.13
4	75,011	6.88
5	138,660	7.13
6	47,240	7.13
7	47,675	7.13
8	47,305	7.13
9	47,374	7.13
10	45,513	7.13

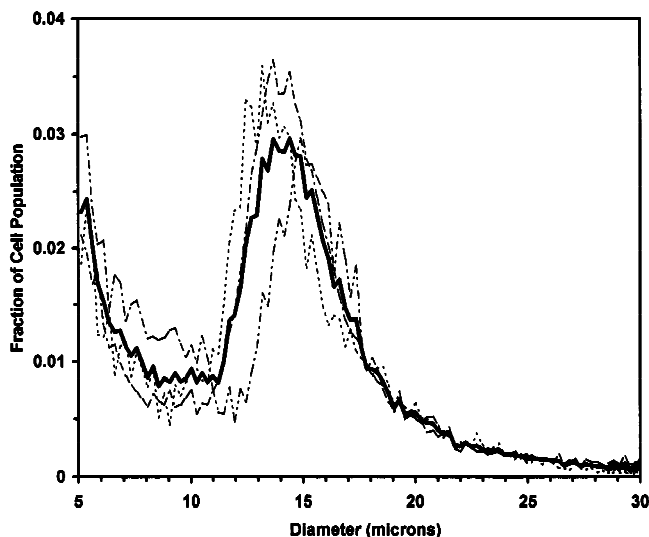


Figure 6. Histograms of the fraction of cell population with a given cell diameter, normalized to the total cell count, for 2C4 cells for Runs A, B, and C (dotted lines) and the mean of the three runs (solid line).

primary peak in each figure. With the human lymphocytes, the second, smaller, peak at approximately 1.2×10^{-2} mm/s is most probably the result of clumps of cells, which were also observed visually.

DISCUSSION

The primary goal of this paper is to demonstrate the ability and accuracy of the experimental device and the computer algorithms to determine cell size by experimentally determining cell settling velocity. By rewriting Eq. (1) in terms of cell diameter as a function of settling velocity, one obtains

$$D_c = \left[\frac{18\eta v_t}{g(\rho_c - \rho)} \right]^{1/2}, \quad (4)$$

where D_c is the cell diameter. Figure 9 is a graphical representation of Eq. (4), plotting cell diameter as a function of velocity, using the following constants: 9.8 m/s^2 for gravity, $1 \times 10^{-3} \text{ Pa-s}$ for η , and 0.054 for the density difference, $(\rho_c - \rho)$, between the sphere and suspending fluid. This density difference was calculated by using a value of 1.07 for the specific gravity of human lymphocytes, which are reported to range between 1.065 and 1.075 (Sanderson, 1982), and the experimentally determined density of the suspending buffer of 1.016 g/cm^3 ($1.016 \times 10^3 \text{ kg/m}^3$). Note the non-linear nature of the relationship with a greater sensitivity of the cell diameter with respect to settling velocity (more rapid change) for low values of settling velocity.

The resolution of computer imaging techniques, such as those used in the technique discussed in this paper, are dependent on the real world dimensions of the smallest video picture element, the pixel. In the current application, a microscope objective of $5\times$, a photoeyepiece of 2.5 or

Table IV. Results of Coulter counter (Multisizer Iie) analysis of 2C4 cells.

Run	No. of cells	Mean diameter (microns)	Standard deviation (microns)
A	18,748	15.30	3.5
B	64,593	15.56	3.49
C	10,970	16.07	3.71

$6.7\times$, and a computer digitizing board resolution of 624×450 were used. This corresponds to each pixel having dimensions of $2.59 \times 2.57 \text{ }\mu\text{m}$ using the $5\times$ objective and $0.957 \times 0.955 \text{ }\mu\text{m}$ using the $6.7\times$ objective. If a single, $7.1\text{-}\mu\text{m}$ lymphocyte is correctly identified and imaged, it would appear to have a diameter of 3 pixels using the $5\times$ objective or 7 pixels using the $6.7\times$ objective. To obtain a single velocity data point, the CTV computer algorithm requires that a cell had to be tracked in at least five consecutive frames. While the images were recorded at a rate of 30 frames per second, to detect significant movement we used every 20th frame for analysis. Consequently, the time interval between frames used for analysis was 0.667 s. This corresponds to a total time increment of 2.67 s over the 5 frames. During these 2.67 s, a $7\text{-}\mu\text{m}$ cell would move $3.84 \text{ }\mu\text{m}$, while a $7.5\text{-}\mu\text{m}$ cell would move $4.41 \text{ }\mu\text{m}$ which corresponds to a difference of $0.566 \text{ }\mu\text{m}$. On average, it should be possible to detect a difference in location greater than $0.5 \text{ }\mu\text{m}$ if the $6.7\times$ objective was used. This indicates that it is theoretically possible to determine a difference in cell size of $0.5\text{-}\mu\text{m}$ for cells $7 \text{ }\mu\text{m}$ in diameter. In contrast, because of the nonlinear nature of the relationship and the higher settling speed of larger cells, it is theoretically possible to determine the difference in cell size of $0.3 \text{ }\mu\text{m}$ for cells $14 \text{ }\mu\text{m}$ in diameter.

One measure of the experimental accuracy of this approach is to compare the results to cell diameters determined using the Coulter counter. As Fig. 5 indicates, a

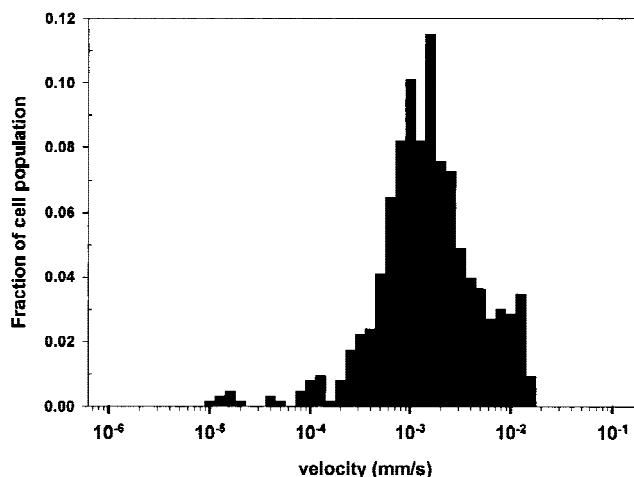


Figure 7. Histogram of the fraction of the cell population with a given settling velocity for human lymphocytes, $n = 637$.

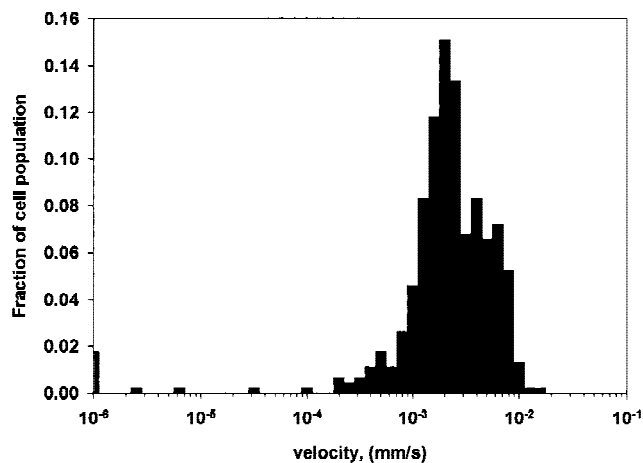


Figure 8. Histogram of the fraction of the cell population with a given settling velocity for 2C4 fibrosarcoma cells, $n = 457$.

relatively large variability in the distribution in diameters of Ficoll–Paque-separated human lymphocytes was observed using the Coulter counter. The greatest reason for this variability appears to be due to variability between donors, since the five runs on the same donor produced the dotted lines which, effectively, lie on top of each other. In “Lymphocytes: A Practical Approach” (Klaus, 1987) it is reported that the volume of lymphocytes can range from 120 to 290 μm^3 . If it is assumed that a lymphocyte is a perfect sphere, this corresponds to a range in diameters of 6.1 to 8.2 μm . The results presented in Fig. 5 are consistent with that report.

To facilitate the comparison between the Coulter counter data on cell diameters with the calculated cell diameters from the experimentally determined settling velocities, a histogram was created and is presented in Fig. 10. To further facilitate this comparison, the same bin size was selected for both sets of data. As can be observed, the data from the CTV experiments indicates a significantly larger number of cells of diameters greater than 10 μm . We believe this is the result of cell clumping which we qualitatively observed in the video images.

Figure 11 is a histogram of the diameters of 2C4 cells as determined by the Coulter counter and the CTV system. Again, the histogram of cell size distribution from settling velocities was calculated using the same range of diameters and bin sizes as was used by the Coulter counter. Unfortunately, unlike the human lymphocytes, no data could be found for the density of 2C4 cells. Consequently, a range of

Table V. Results of settling velocity determinations using computer imaging/particle tracking velocimetry technique.

Cells	No. of cells tracked	Mean velocity (mm/s)	Standard deviation (mm/s)
Lymphocytes	637	2.55×10^{-3}	2.39×10^{-3}
2C4	457	2.75×10^{-3}	2.11×10^{-3}

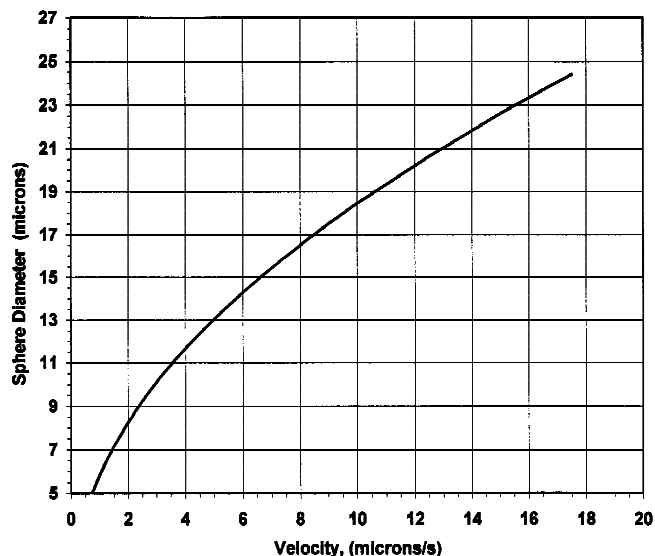


Figure 9. Plot of sphere diameter as a function of velocity using Stokes settling velocity relationship.

densities was empirically tested, and the best fit was obtained using a density of 1.036 g/cm^3 for 2C4 cells. Again, as with the lymphocytes, the CTV data indicates a higher proportion of large cells compared to the Coulter counter data. The relationship used to relate cell diameter to experimentally determined settling velocity (Eq. (4)) has several significant assumptions. First, it assumed that the densities of the cells are constant from cell to cell and, second, that the cell diameter can be represented as a perfect sphere. As presented previously, between different types of cells significant differences in density have been reported. However, as was also reported, within a well-defined cell type (i.e., CFU-GM) a very small distribution in densities has been reported. Consequently, it is highly probable that a small distribution in densities existed in both the cell types studied

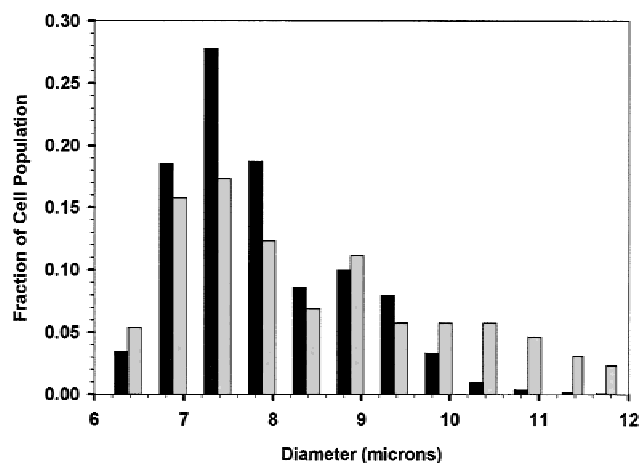


Figure 10. Histogram comparing the distribution of the diameters of human lymphocytes determined from averaged Coulter counter data (black bars) and experimentally determined settling velocity and Stokes law (gray bars).

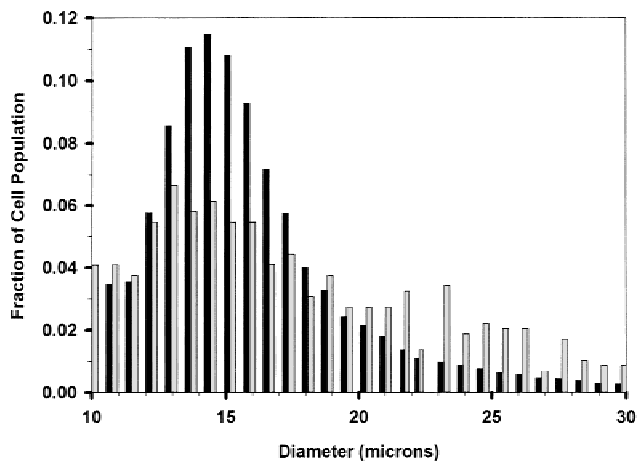


Figure 11. Histogram comparing the distribution of the diameters of CD2 fibrosarcoma cells determined from averaged Coulter counter data (black bars) and experimentally determined settling velocity and Stokes law (gray bars).

in this work. With respect to the effect of a nonspherical cell shape on the calculation of cell diameter from settling velocity measurements, Meistrich (1983) states that shape factors do not vary much between different types of cells, and even in an extreme case, such as for erythrocytes, which are ellipsoid, only a 10% effect is observed. Also, Bertonecello (1987), when comparing unit gravity sedimentation and centrifugal elutriation, states that shape factors may play a significant role in centrifugal elutriation, when compared to unit gravity sedimentation, since cells are placed under significant conformational stress as compared to the gentle forces in unit gravity sedimentation.

A number of improvements in this system are being implemented and/or considered. First, if higher magnification is used, it will be possible, on a cell-by-cell basis, to measure both the cell diameter and density (through settling velocity measurements). This will directly address the two major assumptions spoken of above. The authors are not aware of any other system that will have such a capability. Second, if a longer time gap between images is used, it will be possible to improve the size resolution (ability to distinguish small differences in diameters). Finally, issues surrounding cell clumping will be addressed.

This paper, the first in a two part series, demonstrates the potential of using cell tracking velocimetry of microscopic images of individual cells to determine cellular properties from the movement of cells in an external field. The next paper will discuss the use of this technique to calculate the magnetic susceptibility of individual, immunomagnetically labeled cells in well-defined magnetic energy gradients.

The authors express their thanks to the National Science Foundation (Grant No. BCS 9258004), the National Institutes of

Health (Grant No. CA 62349), and the Whitaker Foundation (Grant No. 20010308) for their financial support.

References

- Bertoncello I. 1987. A comparison of cell separations obtained with centrifugal elutriation and sedimentation at unit gravity. In: Pretlow TG, II, Pretlow T, editors. Cell separation methods and selected applications. San Diego: Academic Press. p 89–108.
- Bikoue A, George F, Poncelet P, Mutin M, Janossy G, Sampol J. 1996. Quantitative analysis of leukocyte membrane antigen expression: normal adult values. *Cytometry* 26:137–147.
- Chalmers JJ, Mandal S, Fang B, Sun L, Zborowski M. 1998. Theoretical analysis of cell separation based on cell surface marker density. *Biotechnol Bioeng* 59:10–20.
- Chalmers J, Zborowski M, Sun L, Moore L. 1998. Flow through, immunomagnetic cell separation. *Biotechnol Prog* 14:141–148
- Guezennec YG, Brodkey RS, Trigui N, Kent JC. 1994. Algorithms for fully automated three-dimensional particle tracking velocimetry. *Exp Fluids* 17:209–219.
- Han Y, Watling D, Rogers NC, Stark G. 1997. JAK2 and Stat5, but not JAK1 and Stat1, are required for prolactin-induced β -lactoglobulin transcription. *Mol Endocrinol* 11:1180–1188.
- Klaus GGB. 1987. *Lymphocytes: A practical approach*. Oxford: IRL Press.
- Lasky LC, Zanjani ED. 1985. Size and density characterization of human committed and multipotent hematopoietic progenitors. *Exp Hematol* 13:680–684.
- Meistrich ML. 1983. Experimental factors involved in separation by centrifugal elutriation. In: Pretlow TG, II, Pretlow T, editors. Cell separation methods and selected applications. San Diego: Academic Press. p 33–61.
- Reddy S, Moore L, Zborowski M, Chalmers JJ. 1996. Determination of the magnetic susceptibility of labeled particles by video imaging. *Chem Eng Sci* 51:947–956.
- Sanderson R. 1982. Separation of different kinds of nucleated cells from blood by centrifugation elutriation. In: Pretlow TG, II, Pretlow T, editors. Cell separation methods and selected applications. San Diego: Academic Press. p 153–154.
- Shapiro H. 1995. *Practical flow cytometry*. 3rd ed. New York: Wiley-Liss. p 232.
- Sun L, Zborowski M, Moore L, Chalmers JJ. 1998. Continuous, flow-through immunomagnetic cell separation in a quadrupole field. *Cytometry* 33:469–475.
- Terstappen LW, Mickaels RQ, Dost R, Loken MR. 1990. Increased light scattering resolution facilitates multidimensional flow cytometric analysis. *Cytometry* 11:506–512.
- Venkat RV, Chalmers JJ. 1996. Characterization of agitation environments in 250 mL spinner vessel, 3 L, and 20 L reactor vessel used for animal cell microcarrier culture. *Cytotechnology* 22:95–102.
- Venkat R, Stock R, Chalmers JJ. 1996. Study of hydrodynamics in microcarrier culture spinner vessels: A particle tracking velocimetry approach. *Biotechnol Bioeng* 49:456–466.
- Watling D, Guschin D, Muller M, Silvennoinen O, Witthuhn B, Quelle FW, Rogers NC, Schindler C, Stark GR, Ihle JN, Kerr IM. 1993. Complementation by the protein tyrosine kinase JAK2 of a mutant cell line defective in the interferon- γ signal transduction pathway. *Nature* 366:166–170.
- Zborowski, M., Moore, L.R., Sun, L., Chalmers, J.J., 1997. Continuous-flow Magnetic Cell Sorting Using Soluble Immunomagnetic Labels, In: Scientific and Clinical Applications of Magnetic Carriers, W. Schuett, U. Hafeli, J. Teller, M.Zborowski eds. Plenum Press.
- Zborowski, M., Fuh, C.B., Green, R., Sun, L., Chalmers, J.J., 1995. Analytical Magnetopheresis of Ferritin-labeled Lymphocytes, *Anal. Chem.* 67:3702–3712.